Hover Dynamics & Flight Control of a UAM-Scale Quadcopter with Hybrid RPM & Collective Pitch Control

Ariel Walter PhD Student
Michael McKay PhD Graduate
Robert Niemiec Research Scientist
Farhan Gandhi Redfern Professor, Director
Center for Mobility with Vertical Lift (MOVE)
Rensselaer Polytechnic Institute
Troy, NY, United States

Tom Berger
Flight Controls Group Lead
US Army Combat Capabilities Development Command
Aviation & Missle Center
Moffett Field, CA, United States

ABSTRACT

Hover trim and dynamic analyses were performed on a UAM-scale quadcopter with both variable rotor speed and variable collective blade pitch. The bare-airframe dynamics were first considered at three different hover trim points, where power consumption is increased to improve authority. The control and stability derivatives were examined at each trim point and an increase in base RPM caused increased authority for pitch inputs (and decreased authority for RPM inputs) in thrust-dominated axes. Explicit model following control laws wre then optimized using CONDUIT® to meet ADS-33E-PRF handling qualities specifications. Design margin optimization was then performed on each axis. Heave and yaw responses of the linearized system were examined for the three trim points with either RPM or pitch control. It was found that pitch-control outperformed RPM-control in heave, while the opposite was true for yaw. Hybrid control mixing was considered using a complementary filter, so that it uses pitch actuators for short-term responses, and RPM for trim. Effects of changes in motor time constant and complementary filter cutoff frequency were examined. The benefits of hybrid control were demonstrated through simulations that involved transition between trim points. Hybrid control required lower maximum power during thrust-driven maneuvers by allowing the aircraft to accelerate using pitch actuators, and recovers the original stall margin by using the rotor speed to re-trim. For a drop-off of 176 lbs of payload, hybrid control provided 5.0% lower trim power than pitch control with the reduced weight. Hybrid control also allowed a 3.9% reduction in power compared to pitch control at a flight speed of 30 kts.

NOTATION

Symbols

K	Input Scaling
p	Roll Rate, Body Axis
q	Pitch Rate, Body Axis
r	Yaw Rate, Body Axis
t	Time
T	Time Delay
u	Longitudinal Velocity, Body Axis
U	Control Inputs
v	Lateral Velocity, Body Axis
V	Motor Voltage
w	Heave Rate, Body Axis
X	Dynamic States
α	Complementary Filter Cutoff Frequency
δ	Acceleration Input
θ	Pitch Attitude
Θ	Blade Root Pitch
τ	Time Constant
ϕ	Roll Attitude
ψ	Heading
Ψ	Azimuthal Location
ω	Natural Frequency
Ω	Rotor Speed
ζ	Damping Ratio

Acronyms

ACAH	Attitude Command, Attitude Hold
DMO	Design Margin Optimization
EMF	Explicit Model Following
eVTOL	Electric Vertical Takeoff and Landing
MRC	Multi-Rotor Coordinate
OLOP	Open-Loop-Onset-Point
RMS	Root Mean Square
RPM	Revolutions Per Minute
UAM	Urban Air Mobility

Presented at the Vertical Flight Society's 78th Annual Forum & Technology Display, Ft. Worth, Texas, USA, May 10–12, 2022.
Copyright © 2022 by the Vertical Flight Society. All rights reserved.
Distribution Statement A: Approved for public release. Distribution is unlimited.

INTRODUCTION

As development of electric Vertical Takoff and Landing (eVTOL) platforms for Urban Air Mobility (UAM) applications progresses, many challenges must be overcome. It has previously been found (Refs. 1–5) that UAM-scale multicopters that rely exclusively on fixed-pitch, variable-RPM rotors for control may struggle to meet standard handling qualities specifications without relatively over-sized electric motors. This has been shown to be driven by spikes in motor current that are needed as the controller must overcome the rotor inertia and rapidly change the rotor speeds in order to produce the changes in thrust needed to maneuver the aircraft and provide satisfactory responsiveness.

Another option for control of multirotor aircraft is the use of variable collective pitch of the rotors. Like the collective feathering used for conventional VTOL aircraft, varying the blade pitch allows for changes in thrust without accelerating the rotors. In Ref. 3, Malpica and Withrow-Maser found that UAM-scale aircraft with collective pitch control were able meet handling qualities parameters, but aircraft with rotor speed control could not (with the assumed drivetrains). Niemiec et al. (Ref. 5) also considered both rotor speed and collective pitch control, but found that both configurations were limited by the current requirements for yaw maneuvers, as these relied directly on motor torque, which is proportional to current.

Theron et al. (Ref. 6) previously considered a hybrid variable-RPM and variable-collective-pitch control scheme for a UAM-scale eVTOL aircraft using nonlinear dynamic inversion. Utilizing a complementary filter for control mixing between variable-RPM and variable-pitch, the hybrid control scheme did not provide any benefit over the collective pitch control scheme. However, this study did not perform optimization of the control algorithm and only examined a subset of the standard handling qualities requirements defined in the ADS-33E-PRF (Ref. 7).

It has previously been shown by McKay et al. (Ref. 8) that variable-RPM control is more power efficient than variable-pitch control when considering changes in trim condition. The use of hybrid RPM and collective pitch control will allow the aircraft to utilize the faster pitch actuators for maneuvers and short-term responses, while allowing the utilization of changes in rotor speeds for long-term responses, such as trim.

The goal of this study is to analyze the dynamics of a UAM-scale eVTOL quadcopter with hybrid variable-RPM and variable-pitch control. Since the aircraft has redundant controls, several trim points can be considered, and the resulting changes in linear dynamics analyzed. Then, optimized Explicit-Model-Following (EMF) controllers can be designed using CONDUIT® to meet standard ADS-33E-PRF (Ref. 7) handling qualities specifications. Aircraft performance will then be compared with either variable-RPM control, variable-pitch control, or a combination of both utilizing a complementary filter for control mixing.

MODELING AND ANALYSIS

Platform

A hybrid variable-RPM and variable-pitch control scheme is applied to a UAM-scale (1200 lb gross weight) quadcopter, the same platform as is used in Refs. 2 & 9. Basic aircraft parameters are listed in Table 1 and fuselage inertia is scaled from the 1-passenger NASA concept quadcopter (Ref. 10). As shown in Fig. 1, the quadcopter is flown in an edge-first orientation with the rotors spaced to allow a tip clearance of 10% of the rotor radius.

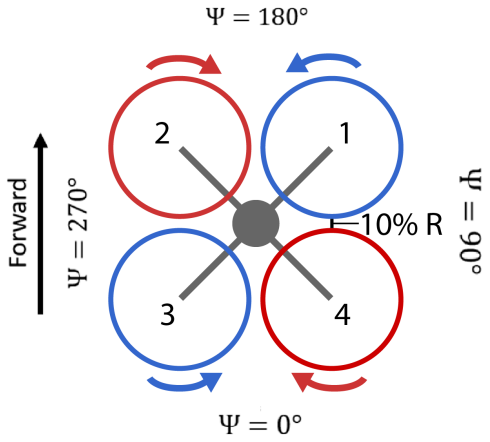

Figure 1: Quadcopter Configuration

Table 1: Aircraft Parameters

Parameter	Value
Gross Weight	1200 lb
Disk Loading	6 psf
Rotor Radius	4 ft
Rotor Inertia	47 lb ft^2
Blade Twist	-10.3°

Simulation Model

Nonlinear dynamic simulation models are generated using the Rensselaer Multicopter Analysis Code (RMAC, Ref. 11). Within RMAC, each rotor is modeled using blade element theory, coupled to a 10-state Peters-He dynamic wake model (Ref. 12). The motor dynamics are modeled using DC motor equations, assuming zero motor inductance (with motor parameters derived as in Ref. 3).

With both variable RPM and variable collective pitch control on each of the four rotors, the aircraft has 8 control inputs. Control mixing is achieved via a multi-rotor coordinate transform (Ref. 13). In multi-rotor coordinates, the inputs to the aircraft model are

$$U = [V_0 \; V_{1s} \; V_{1c} \; V_d \; \Theta_0 \; \Theta_{1s} \; \Theta_{1c} \; \Theta_d]^T \quad (1)$$

Thus, each aircraft axis (heave, roll, pitch, and yaw) is affected by exactly two control inputs, one associated with rotor speed (V), and one with blade pitch (Θ). The transform between multirotor and individual rotor coordinates (numbered as in Fig. 1) for the motor speed inputs is

$$\begin{bmatrix} V_1 \\ V_2 \\ V_3 \\ V_4 \end{bmatrix} = \begin{bmatrix} 1 & \sin(\Psi_1) & \cos(\Psi_1) & 1 \\ 1 & \sin(\Psi_2) & \cos(\Psi_2) & -1 \\ 1 & \sin(\Psi_3) & \cos(\Psi_3) & 1 \\ 1 & \sin(\Psi_4) & \cos(\Psi_4) & -1 \end{bmatrix} \begin{bmatrix} V_0 \\ V_{1s} \\ V_{1c} \\ V_d \end{bmatrix} \quad (2)$$

where Ψ_i is the rotor hub azimuthal location. The same transform is used for the pitch inputs.

The full linearized dynamics model includes 56 states: 12 rigid body states, 4 rotor speeds in multirotor coordinates, and 10 inflow states per rotor. The high frequency inflow states can be reduced out by static condensation, leaving a 16-state system:

$$X = [x \; y \; z \; \phi \; \theta \; \psi \; u \; v \; w \; p \; q \; r \; \Omega_0 \; \Omega_{1s} \; \Omega_{1c} \; \Omega_d]^T \quad (3)$$

Control Architecture

As has been done previously (Ref. 1), an Attitude-Command-Attitude-Hold/Rate-Command-Direction-Hold (ACAH/RCDH) explicit-model-following (EMF) control architecture is utilized to stabilize and control the aircraft in hover (Fig. 2).

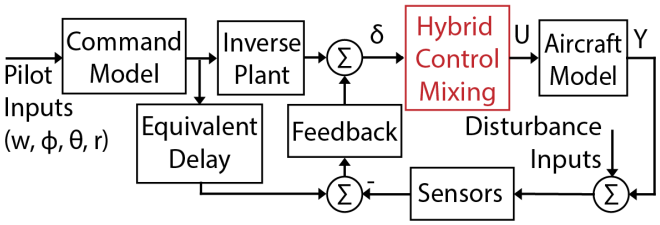

Figure 2: EMF Control Architecture

Pilot inputs are first passed through a command filter (first-order filter for heave and yaw, second-order filter for roll and pitch). The feedforward path consists of an approximate inverse of the aircraft model, and the feedback path includes an equivalent delay that approximates the effects of the dynamics excluded from the inverse model approximation, including actuator and sensor dynamics. A senor delay of 25 ms is included on the output signals from the simulation model (as described in Ref. 14).

The sum of the feedforward and feedback paths is not specifically a rotor speed or blade pitch input, but rather treated as an acceleration command δ for each axis:

$$\delta = [\delta_0 \;\; \delta_{1s} \;\; \delta_{1c} \;\; \delta_d].^T \quad (4)$$

This allows each aircraft axis to be treated as a Single-Input-Single-Output (SISO) system despite having two control inputs (motor voltage and collective blade pitch in multirotor coordinates). Control mixing for the hybrid control system takes in this input acceleration command for each axis and outputs both the motor voltages (RPM-control) and blade pitches (pitch-control) to give input U (Eq. 1) to the simulation model.

The hybrid control mixing is illustrated by the block diagram in Fig. 3. The acceleration command δ for each multi-rotor input (m) is split into two paths: one corresponding to the rotor speed control path and the other corresponding to the blade pitch control path. Appropriate scaling is applied to the acceleration command based on the bare-airframe dynamics (explained in the next section) and then passed through a complementary filter.

The complementary filter separates the signal into high- and low-frequency content, taking the form

$$\text{High Pass Filter} = \frac{s}{s+\alpha}, \quad \text{Low Pass Filter} = \frac{\alpha}{s+\alpha}. \quad (5)$$

For each rotor, the blade pitch actuator receives the high-frequency (maneuver) content, while the low-frequency (trim) content is allocated to the motor speed controller. This will essentially allow the aircraft to use changes in blade pitch for short-term responses, such as the acceleration at the beginning of a maneuver, and the rotor speed for longer responses, such as changes in trim condition.

The complementary filter cutoff frequency α dictates the frequency at which the transition from RPM-control to pitch-control occurs. In order to illustrate the division between high-frequency and low-frequency content, the frequency response of a complementary filter with $\alpha = 1$ is shown in Fig. 4. When summed together, the high pass and low pass filters result in 0 dB (unity) gain and 0 degrees phase lag.

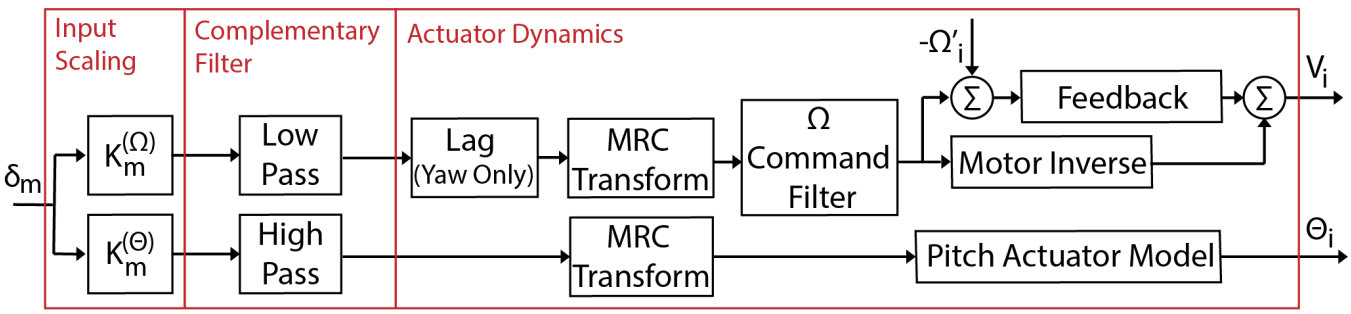

Figure 3: Hybrid Control Mixing and Actuator Dynamics

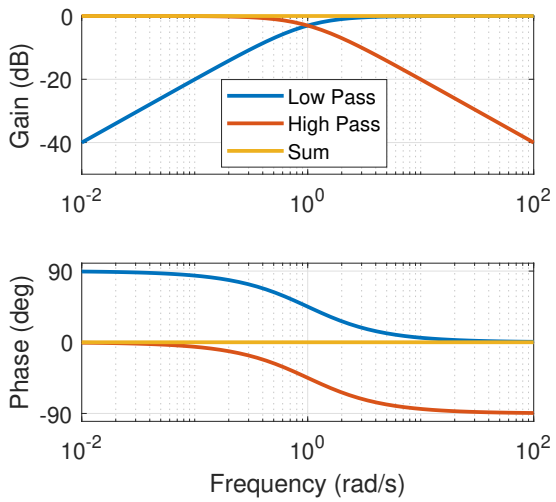

Figure 4: Complementary Filter

Figure 5 demonstrates how the rotor speed and blade pitch inputs are affected by the cutoff frequency of the hybrid controller when commanding an increase in rotor thrust. First considering pure pitch control ($\alpha = 0$, blue in Fig. 5), changes in blade pitch are used for all control while the rotor speed is held at the nominal value. With increasing α, the rotor speed will be used to respond to higher frequency input. With low cutoff frequency ($\alpha = 0.1$, red Fig. 5), the pitch actuator is used for the initial response, but as the simulation progresses, the rotor speed slowly increases while the blade pitch decreases to maintain the desired thrust until the blade pitch has been reduced to its nominal value. This transition happens more rapidly as α increases. As α approaches infinity, the pitch actuator is essentially unperturbed and the change in thrust is produced purely with changes in rotor speed.

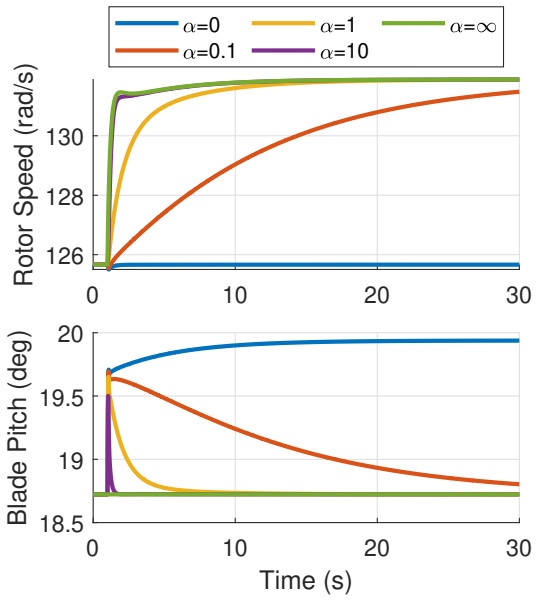

Figure 5: Rotor Speed and Blade Pitch with Hybrid Control

After passing through the complementary filter, both paths are transformed into individual rotor coordinates. The yaw rotor speed path also passes through a lag filter in order to account for additional bare-airframe dynamics (see later section).

Another EMF control loop is implemented on the rotor speed. Though the motor dynamics can be perfectly inverted and feedfoward control alone is sufficient (Ref. 15), feedback control on the rotor speed in also included in order to account for changes in rotor speed that occur when the blade pitch changes. This is used to drive the change in rotor speed to zero when pure collective-pitch control is being considered.

Pitch actuator dynamics are included in the blade pitch control path. The actuator is assumed to be second-order,

$$G_\theta = \frac{\Theta}{\Theta_{cmd}} = \frac{\omega_N^2}{s^2 + 2\zeta\omega_N s + \omega_N^2} \tag{6}$$

with an assumed damping ratio of $\zeta = \sqrt{2}/2$ and natural frequency of $\omega_N = 60$ rad/s. The pitch actuator also includes a rate limit of 20 deg/s and limits the actuator position to a maximum of 24 degrees to avoid potential stall.

The input voltages and blade pitches for each individual rotor (i) are output from the hybrid control mixer. These inputs are transformed to multi-rotor coordinates via an inversion of the transform in Eq. 2 before being input to the aircraft simulation model.

Hover Dynamics & Input Scaling

Scaling of the acceleration inputs for each axis is determined based on analysis of the bare-airframe dynamics, with the assumption of the rotor speed control loop being closed. With the use of multirotor coordinates, the linearized hover model can be split into independent models for each axis, each with two inputs. The dynamics of each axis are broken down to examine the sensitivity to changes in rotor speed or blade pitch and determine appropriate input scaling (from Fig. 3).

The heave dynamics can be represented by

$$\begin{bmatrix} \dot{w} \\ \dot{\Omega}_0 \end{bmatrix} = \begin{bmatrix} Z_w & Z_\Omega \\ T_w & T_\Omega \end{bmatrix} \begin{bmatrix} w \\ \Omega_0 \end{bmatrix} + \begin{bmatrix} 0 & Z_\theta \\ T_V & T_\theta \end{bmatrix} \begin{bmatrix} V_0 \\ \theta_0 \end{bmatrix} \tag{7}$$

with the heave rate and collective rotor speed as states and the collective voltage and collective blade pitch as inputs. The collective rotor torque produced from changes in heave rate (T_w) and from changes in collective blade pitch (T_θ) are negligible. Thus, the heave model can be simplified to get

$$\dot{w} = Z_w w + Z_\Omega \Omega_0 + Z_\theta \theta_0. \tag{8}$$

From these simplified dynamics (without considering actuator dynamics), the main difference between the heave response w from changes in rotor speed versus changes in blade pitch is a difference in gain (Z_Ω versus Z_Θ). Thus, the inverse of these values is used to scale the heave acceleration input for the corresponding control path.

The linearized pitch dynamics model is

$$\begin{bmatrix} \dot{\theta} \\ \dot{u} \\ \dot{q} \\ \dot{\Omega}_{1c} \end{bmatrix} = \begin{bmatrix} 0 & 0 & 1 & 0 \\ -g & X_u & X_q & 0 \\ 0 & M_u & M_q & M_\Omega \\ 0 & 0 & T_q & T_\Omega \end{bmatrix} \begin{bmatrix} \theta \\ u \\ q \\ \Omega_{1c} \end{bmatrix} + \begin{bmatrix} 0 & 0 \\ 0 & 0 \\ 0 & M_\theta \\ T_V & T_\theta \end{bmatrix} \begin{bmatrix} V_{1c} \\ \theta_{1c} \end{bmatrix}. \quad (9)$$

Since the roll and pitch dynamics of the vehicle are nearly identical (the only difference being a difference in fuselage inertia), only the pitch model is presented. Several effects are negligible, and the pitch dynamics can be simplified with the assumption that $X_q = T_q = T_\theta = 0$. Rewriting the third row of Eq. 9 gives

$$\dot{q} = M_u u + M_q q + M_\Omega \Omega_{1c} + M_\theta \theta_{1c}. \quad (10)$$

From this, the difference in gain between pitch response from changes in rotor speed versus changes in blade pitch (M_Ω versus M_Θ) can again be identified, with the inverse values used to scale the pitch acceleration input.

The linearized yaw dynamics include the yaw rate and differential rotor speed as states and the differential motor voltage and differential blade pitch as inputs:

$$\begin{bmatrix} \dot{r} \\ \dot{\Omega}_d \end{bmatrix} \begin{bmatrix} N_r & N_\Omega \\ T_r & T_\Omega \end{bmatrix} \begin{bmatrix} r \\ \Omega_d \end{bmatrix} + \begin{bmatrix} N_V & 0 \\ T_V & T_\theta \end{bmatrix} \begin{bmatrix} V_d \\ \theta_d \end{bmatrix}. \quad (11)$$

The yaw dynamics differ notably from the heave and pitch axes in two ways:

1. The pitch input does *not* have a direct impact on the yaw acceleration of the vehicle. The only way a pitch input can produce a yaw moment is indirectly through the motor dynamics. Thus, the effect of rotor pitch on the rotor speed cannot be safely ignored.

2. The motor voltage has a direct effect on the yaw rate. Thus, when Ω_d is commanded, and V_d rises to meet that command, the vehicle will yaw immediately, leading the motor response.

Thus, the yaw axis must be handled differently than the thrust-dominated axes.

Of all of the derivatives in Eq. 11, only the effect of yaw rate on rotor acceleration, T_r, can be neglected. Input scaling parameters can be obtained by assuming perfect tracking of Ω_d ($\Omega_d = \Omega_{d,cmd}$). The second row of Eq. 11 becomes

$$\begin{aligned} 0 &= T_\Omega \Omega_{d,cmd} + T_\theta \theta_d + T_V V_d \\ V_d &= -\frac{T_\Omega \Omega_{d,cmd} + T_\theta \theta}{T_V} \end{aligned} \quad (12)$$

Substitution into the first row of Eq. 11 yields

$$\dot{r} = N_r r + \left(N_\Omega - \frac{N_V T_\Omega}{T_V} \right) \Omega_{d,cmd} - \frac{N_V T_\theta}{T_V} V_d \quad (13)$$

To account for the direct effect of voltage on yaw rate, consider the transfer function from commanded differential RPM $\Omega_{d,cmd}$ to yaw rate r, which takes the form

$$\frac{r}{\Omega_{d,cmd}} = \frac{N_V}{T_V} \left(s + \frac{T_V N_\Omega - T_\Omega N_V}{N_V} \right) C_\Omega \frac{1}{s - N_r} \quad (14)$$

where the zero represents the lead introduced by the voltage's immediate effect on the motor reaction torque and C_Ω represents the motor speed command filter in Fig. 3. By adding a lag filter to cancel out the zero, the yaw response becomes a simple first-order transfer function, multiplied by the rotor speed command model. A summary of the input scaling for the yaw axis, as well as others is presented in Table 2.

Table 2: Input Scaling

	Heave	Roll	Pitch	Yaw
$K^{(\Omega)}$	$1/Z_\Omega$	$1/L_\Omega$	$1/M_\Omega$	T_V/N_V
$K^{(\Theta)}$	$1/Z_\Theta$	$1/L_\Theta$	$1/M_\Theta$	$-T_V/(N_V T_\Theta)$

Hybrid Control Mixing

A key component of the EMF control architecture (Fig. 2) is the approximation of the inverse model. This approximation is relatively straightforward when considering pure RPM or pitch control. For example, considering the heave axis with RPM-control, the model inversion uses the heave damping (Z_w), a gain (Z_Ω), and an equivalent delay to approximate the effects of the actuator dynamics (Ω/V).

When considering hybrid control, the inverse model must approximate the needed acceleration command δ to produce the desired vehicle response. Both the RPM and pitch control paths contribute to this and affect the approximation. Again using the heave axis as an example, the block diagram shown in Fig. 3 combined with the aircraft model can be represented as a transfer function:

$$\begin{aligned} G_0 &= \frac{w}{\delta_0} \\ &= \frac{1}{(s - Z_w)(s + \alpha)} \Bigg(\underbrace{\frac{\alpha}{\tau_\Omega + 1}}_{\text{RPM Path}} + \underbrace{\frac{\omega_N^2 s}{s^2 + \zeta \omega_N s + \omega_N^2}}_{\text{Pitch Path}} \Bigg) \\ &= \frac{1}{(s - Z_w)} \frac{\alpha \tau_\Omega^{-1} (s^2 + 2\zeta\omega_N s + \omega_N^2) + \omega_N^2 s (s + \tau_\Omega^{-1})}{(s + \alpha)(s + \tau_\Omega^{-1})(s^2 + 2\zeta\omega_N s + \omega_N^2)}. \end{aligned} \quad (15)$$

As shown in Eq. 15, the use of the complementary filter will introduce two zeros as well as a pole at the cutoff frequency. As $\alpha \longrightarrow 0$, the motor pole (τ_Ω^{-1}) will reduce out and only the pitch actuator will be used, while as $\alpha \longrightarrow \infty$, the pitch actuator dynamics will cancel and only the rotor speed will be used for control.

The hybrid control model is approximated by

$$\tilde{G}_0 = \frac{1}{(s - Z_w)} e^{-s\mathrm{T}(\alpha, \tau_\Omega)}. \quad (16)$$

With the input scaling from Table 2, the effective gain from the plant is 1. A delay $T(\alpha, \tau_\Omega)$ is included in order to approximate the effects of the mixed motor dynamics and pitch actuator. Since the pitch actuator model is fixed (Eq. 6), the delay is considered a function of the complementary filter cutoff frequency α and motor speed time constant τ_Ω.

Considering different values of α and τ_Ω, the equivalent delay (T) is fit in order to minimize the difference in frequency response between the hybrid control plant (Eq. 15) and the approximation (Eq. 16) for a frequency range of 0.1 to 10 rad/s. The optimized delay is plotted in Fig. 6 where the values are cut off when the model following cost between the plant and approximation exceeds 50, as dictated by guidelines in Ref. 16.

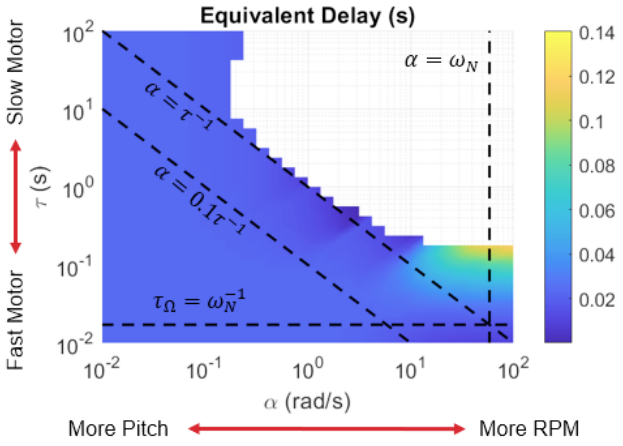

Figure 6: Optimal Equivalent Delay

Several key locations are indicated on Fig. 6 by dashed lines, the significance of which is summarized:

- $\alpha > \omega_N$: Input to the pitch control path is faster than the pitch actuator can adequately follow, effectively reducing the system to only RPM control.
- $\alpha > 0.1\tau_\Omega^{-1}$: Input to the RPM path begins to include content faster than the motor can adequately follow. As α approaches τ_Ω^{-1}, more high-frequency content is routed to the motors that lack the bandwidth to follow.
- $\tau_\Omega < \omega_N^{-1}$: Motor is required to respond faster than the pitch actuator, which is unlikely in practice and will not be considered in this study.

Despite improving motor response times, smaller values of τ_Ω generally lead to higher required motor current as a result of the higher required acceleration. However, values of τ_Ω above $0.1/\alpha$ can cause the zero in Eq. 15 to have more effect on the frequency response, reducing the accuracy of the model approximation. This behavior is illustrated in Fig. 7 for a cutoff frequency of 1 rad/s, and becomes less pronounced at smaller and larger values of α as the system moves more toward pure RPM or pitch control. As α increases past 10 or decreases

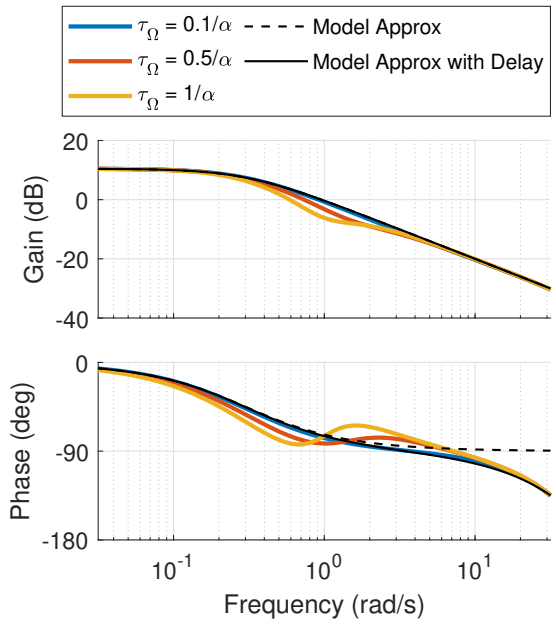

Figure 7: Plant Approximation for $\alpha = 1$

past 0.1, the zero behavior is pushed out of frequency range of interest for model following, so $\tau_\Omega > 0.1\alpha$ can by considered. For $10 > \alpha > 0.1$, model following with $\tau_\Omega > 0.1\alpha$ could be improved by considering a higher-order inverse approximation.

When using primarily pitch control for maneuvers ($\alpha \leq 1$), the value of the motor rise time can be fixed to $0.1/\alpha$. Lowering the value of τ_Ω will have no effect on the system, since the complementary filter will already have filtered out any higher frequency content on the RPM path.

From Fig. 6, the value of the delay for the model approximation is fixed at T=25 ms, as this should provide an adequate model following at high frequency, as long as $\alpha \leq \tau_\Omega^{-1}$. This value is driven by the delay from the pitch actuator, which is used for high-frequency response.

Control Optimization

As recommended in Ref. 14, a standard set of handling qualities specifications are considered as constraints during control optimization, listed in Table 3. The optimization routine seeks minimize the actuator effort (defined by the summed objectives), without violating any hard (stability) or soft (performance) constraints.

In addition to several ADS-33E-PRF (Ref. 7) hover and low speed requirements such as required piloted bandwidth and minimum damping ratios, disturbance rejection requirements (Ref. 17), and Open-Loop Onset Point (OLOP) specifications are also included. In addition to typical actuator RMS objective functions, additional objective functions associated with the motor current during heave, pitch, and yaw step responses are included. This is included with the aim of minimizing the peak current during maneuvers, as well as to impose a limit

Table 3: CONDUIT® Constraints

Specification	Axes
Hard Constraints	
Eigenvalues	All
Stability Margins	All
Nichols Margin	All
Soft Constraints	
Bandwidth/Phase Delay	Roll, Pitch, Yaw
Crossover Frequency	All
Disturbance Rejection Bandwidth	All
Disturbance Rejection Peak	All
Damping	All
Heave Mode	Heave
Model Following	All
OLOP (Pilot/Disturbance)	All
Summed Objectives	
Actuator RMS (Pilot/Disturbance)	All
Crossover Frequency	All
Motor Current Minimization	All

to the maximum current allowed to the motors, which is constrained to be less than the hover current. A step with magnitude of $w = -3.8$ m/s is used for heave, $\phi/\theta = 20$ degrees for roll/pitch, and $r = 20$ deg/s for yaw.

After meeting standard handling qualities metrics, design margin optimization (DMO) is performed by incrementally increasing the requirements in order to produce a family of Pareto-optimal controllers that provide improved maneuverability with minimum increase in actuator activity. For each axis, the design margin is applied to the bandwidth, crossover frequency, and disturbance rejection bandwidth. The design margin is increased until actuator rate (OLOP or maximum current) or position (blade pitch) limits are reached. The margin is then reduced to 70% of the maximum value, as recommended by Ref. 14.

RESULTS

Hover Trim Analysis

In hover, only the collective inputs are used to trim the aircraft. With two inputs governing the heave axis, infinite trim solutions exist. The choice of hover trim point affects the dynamics, control authority, and power consumption of the aircraft.

The hover trim space is explored by sweeping though prescribed rotor speeds, and solving for the required collective motor voltages and blade pitches. Starting at a collective rotor speed corresponding to a tip speed of Mach 0.6 (1620 RPM), the speed is decreased until the required blade pitch becomes high enough to stall. The resulting power for different trim points is plotted in and corresponding root pitches are plotted in Fig. 8. Stall becomes an issue around 24 degree root pitch (1010 RPM) and is chosen as the upper limit of the blade pitch.

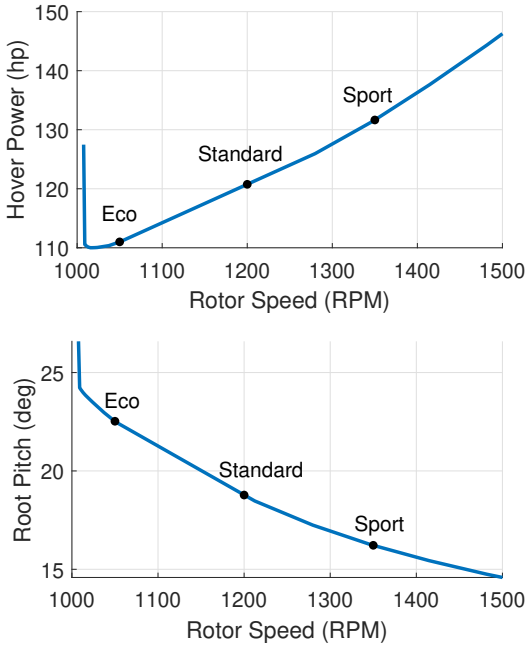

Figure 8: Hover Trim Power and Collective Blade Pitch Input

Some margin needs to be included in hover to avoid stall during maneuvers. An appropriate margin can be estimated from heave bandwidth requirements and an assumed maximum climb rate. Assuming a first-order response type as prescribed by ADS-33E-PRF (Ref. 7), the heave response can be represented by

$$w(t) = w_\infty(1 - e^{-t/\tau}) \tag{17}$$

for commanded heave rate w_∞ and time constant τ. From the derivative of heave rate:

$$\dot{w}(t) = w_\infty(e^{-t/\tau})/\tau \implies \dot{w}_{max} = w_\infty/\tau \tag{18}$$

the maximum heave acceleration is w_∞/τ at $t = 0$. Based on the hover and low speed requirements in ADS-33E-PRF, the maximum allowable heave time constant is $\tau = 5$ seconds. Thus, maximum heave acceleration can be determined by dividing the desired maximum heave rate by τ.

With variable-pitch control during a heave maneuver, the rotors will need to increase their pitch in order to quickly create the additional thrust to accelerate the aircraft upward. Assuming this increase puts the root pitch at 24 degrees, the trim rotor speed is calculated, then the hover trim root pitch is recalculated with this rotor speed. Thus, the hover trim point corresponds to a maximum heave rate. The trim point with the lease stall margin corresponds to a maximum heave rate of 3.8 m/s (760 ft/min), which exceeds the ADS-33E-PRF requirement of 160 ft/min.

Three hover trim points are chosen in order to analyze the differences in heave dynamics (black dots in Fig. 8). Hover trim rotor speeds of 1050 RPM (Eco), 1200 RPM (Standard), and 1350 RPM (Sport) are considered and corresponding blade pitch, hover power, and maximum heave rate (based on estimated thrust increase available with stall margin and maximum heave time constant) are given in Table 4.

Table 4: Hover Trim Points

	Eco	Standard	Sport
Rotor Speed (RPM)	1050	1200	1350
Collective Blade Pitch (deg)	22.5	18.7	16.2
Total Hover Power (hp)	111	121	132
Max Heave Rate (ft/min)	760	4080	7940

These trim points are labeled "Eco", "Standard" and "Sport" based on their trim power consumption. The increase in trim power at higher trim rotor speed comes with an increase in stall margin, and therefore an improvement in expected agility and maneuverability when using pitch control for maneuvers. This difference can be demonstrated by analyzing the bare-airframe dynamics at the different trim points.

Stability & Control Derivatives

Heave First, considering the heave dynamics from Eq. 8, the 2-state, 2-input heave model can be represented by two SISO transfer functions when considering pure RPM or pure blade pitch control. These transfer functions can be further broken down into response (w/Ω_0 or w/Θ_0) and the actuator dynamics (Ω_0/V_0 or $\Theta_0/\Theta_{0,cmd}$):

$$\frac{w}{V_0} \approx \underbrace{\frac{Z_\Omega}{(s+Z_w)}}_{w/\Omega_0} \underbrace{\frac{T_V}{(s+T_\Omega)}}_{\Omega_0/V_0} \tag{19}$$

$$\frac{w}{\Theta_{0,cmd}} \approx \underbrace{\frac{Z_\Theta}{(s+Z_w)}}_{w/\Theta_0} \underbrace{G_\Theta}_{\Theta_0/\Theta_{0,cmd}} \tag{20}$$

The values of the heave stability and control derivatives for each of the hover trim points are given in Table 5. With increasing trim rotor speed, the heave subsidence mode (Z_w) increases in frequency. This is a result of the increased sensitivity of thrust to changes in heave rate at higher rotor speeds.

Table 5: Heave Stability and Control Derivatives

Trim Point	Z_w	Z_Ω	T_Ω	T_V	Z_Θ
Eco	-0.228	-0.184	-15.5	11.7	-0.573
Standard	-0.267	-0.163	-15.2	11.7	-0.834
Sport	-0.312	-0.146	-15.1	11.7	-1.163

At higher trim rotor speed, the heave acceleration (thrust) becomes less sensitive to changes in rotor speed (shown by a reduction in the magnitude of Z_Ω), but more sensitive to changes in collective blade pitch (shown by an increase in magnitude of Z_Θ). This can be seen in the changes in low frequency gain that occur with different trim points (Figs. 9 and 10). With rotor speed control at higher frequency (Fig. 9), the difference between the trim points decreases, due to Z_w scaling similarly to $1/Z_\Omega$. For variable-pitch control (Fig. 10), the difference in gain is consistent across the frequency range.

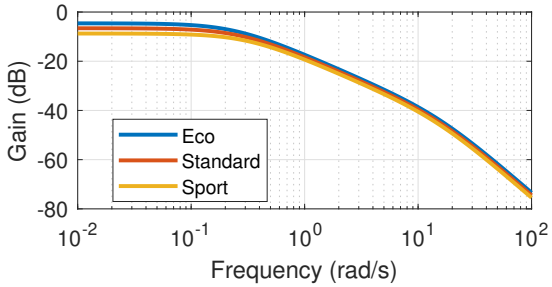

Figure 9: Magnitude Frequency Response of Motor Voltage Input to Heave Rate ($|w/V_0|$)

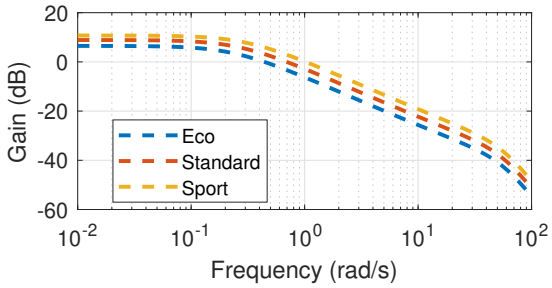

Figure 10: Magnitude Frequency Response of Blade Pitch Input to Heave Rate ($|w/\Theta_{0,cmd}|$)

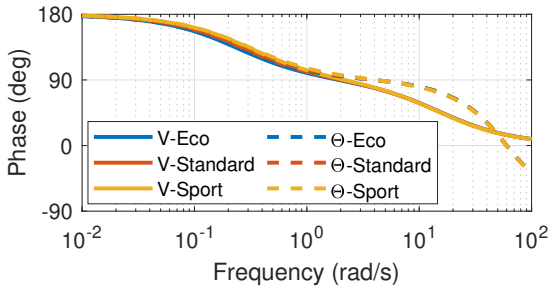

Figure 11: Phase Frequency Response of Collective Input to Heave Rate ($\angle w/V_0$ and $\angle w/\Theta_{0,cmd}$)

The phase of the frequency response (Fig. 11) remains very similar regardless of the trim point, apart from the relative lag between the motor pole and pitch actuator bandwidth. Though the stability derivatives change with trim point, it is not enough to have significant effect on the phase response. The low-frequency phase response is similar regardless of control type, with differences resulting from the actuator. With motor voltage input (rotor speed control), the phase rolls off by 90 degrees due to the motor pole (T_Ω), while with blade pitch control the phase rolls off by 180 degrees (due to the second-order pitch actuator) at the higher frequency of the pitch actuator dynamics (G_Θ).

Roll/Pitch Like heave, the roll/pitch dynamics of the aircraft (Eq. 10) can be represented by two SISO transfer functions when considering pure RPM or pure blade pitch control. The transfer functions for both control types share a pole (p_1), zero

(z_1), and unstable phugoid mode ($s^2 - 2\zeta_{ph}\omega_{ph}s + \omega_{ph}^2$). These transfer functions can be further broken down into response to the control input (θ/Ω_{1c} or θ/Θ_{1c}) and the actuator dynamics (Ω_{1c}/V_{1c} or $\Theta_{1c}/\Theta_{1c,cmd}$):

$$\frac{\theta}{V_{1c}} = \underbrace{\frac{M_\Omega(s+z_1)}{(s+p_1)(s^2-2\zeta_{ph}\omega_{ph}s+\omega_{ph}^2)}}_{\theta/\Omega_{1c}} \underbrace{\frac{T_V}{(s-T_\Omega)}}_{\Omega_{1c}/V_{1c}} \tag{21}$$

$$\frac{\theta}{\Theta_{1c,cmd}} = \underbrace{\frac{M_\Theta(s+z_1)}{(s+p_1)(s^2-2\zeta_{ph}\omega_{ph}s+\omega_{ph}^2)}}_{\theta/\Theta_{1c}} \underbrace{G_\Theta}_{\Theta_{1c}/\Theta_{1c,cmd}} \tag{22}$$

The control and stability derivatives for the roll/pitch axis for each trim point are listed in Table 6. The values of T_Ω and T_V are not listed because they are the same as the values in Table 5.

Table 6: Roll/Pitch Stability and Control Derivatives

Trim Point	X_u	M_u	M_q	M_Ω	M_Θ
Eco	-0.025	0.16	-0.71	-0.17	-0.52
Standard	-0.021	0.17	-0.83	-0.15	-0.75
Sport	-0.018	0.20	-0.97	-0.13	-1.05

Shown in Fig. 12, the pole and zero locations vary with the trim point. The choice of trim point has little effect on the phugoid mode, but does affect the location of the subsidence mode.

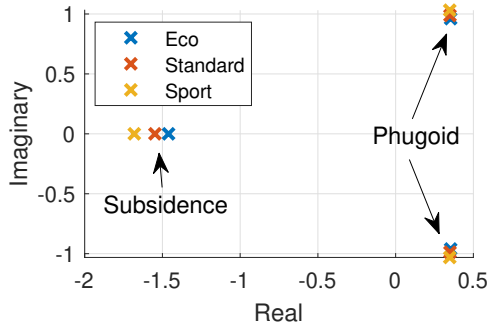

Figure 12: Pole-Zero Map for Bare-Airframe Pitch Dynamics

The trim point also affects the low-frequency gain. At higher rotor speed, the pitch rate becomes less sensitive to rotor speed (M_Ω, Fig. 13), but more sensitive to root pitch (M_Θ, Fig. 14). At very low frequency, this difference is increased by the change in the zero location when considering RPM control (Fig. 13), but reduced when considering pitch control (Fig. 14). The phase response for either control type remains similar regardless of trim point up to the frequency of the actuators (Fig. 15).

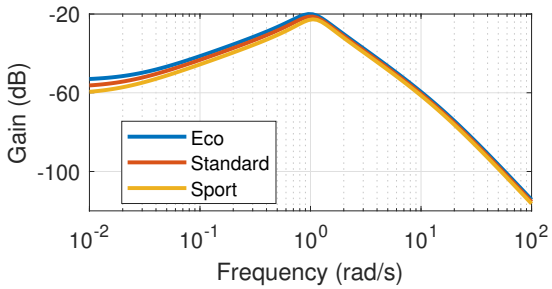

Figure 13: Magnitude Frequency Response of Motor Voltage Input to Pitch Attitude ($|\Theta/V_{1c}|$)

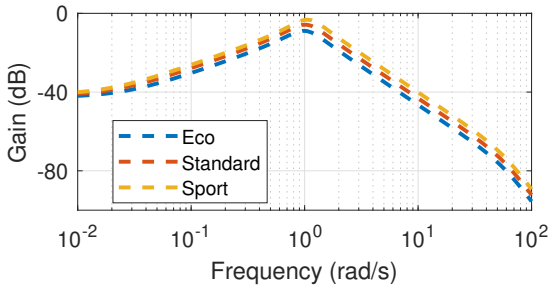

Figure 14: Magnitude Frequency Response of Blade Pitch to Pitch Attitude ($|\theta/\Theta_{1c,cmd}|$)

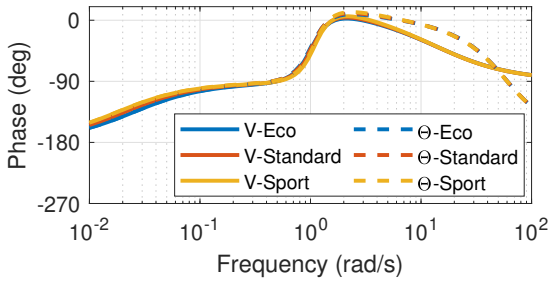

Figure 15: Phase Frequency Response of Longitudinal Input to Pitch Attitude ($\angle\theta/V_{1c}$ and $\angle\theta/\Theta_{1c,cmd}$)

Yaw As mentioned previously during the discussion on input scaling, the yaw dynamics are fundamentally different from the other axes in that it depends on the motors' reaction torque, rather than the rotors' thrust. Since differential voltage, V_d has a direct effect on the yaw acceleration, and an indirect effect via Ω_d, there is a zero in the transfer function r/V_d in addition to the expected two poles.

$$\frac{r}{V_d} \approx \frac{N_V}{(s-N_r)} \frac{(s-T_\Omega+T_V N_\Omega/N_V)}{(s-T_\Omega)} \tag{23}$$

In the absence of motor speed feedback, the rotor pitch has no direct effect on motor torque and, thus, no immediate impact on the yaw acceleration. It does, however, reduce the motor speed via increased aerodynamic torque. This, in turn, reduces the counter-electromotive force produced by the motor, increasing current and reaction torque. Thus, the transfer function r/Θ_d is an over-damped second-order system,

$$\frac{r}{\Theta_{d,cmd}} = \underbrace{\frac{N_\Omega}{(s-N_r)}\frac{T_\Theta}{(s-T_\Omega)}}_{r/\Theta_d}\underbrace{G_\Theta}_{\Theta_d/\Theta_{d,cmd}} \tag{24}$$

The stability and control derivatives for the yaw axis are listed in Table 7. Again, the values T_Ω and T_V are not repeated as the motors are assumed to be identical. For higher trim rotor speed, the yaw rate damping (N_r) becomes smaller, while the reduction in motor speed is more sensitive to changes in pitch as rotor speed increases.

Table 7: Yaw Stability and Control Derivatives

Trim Point	N_r	N_Ω	N_V	T_Θ
Eco (1050 RPM)	-0.050	-0.12	0.11	-6.1
Standard (1200 RPM)	-0.041	-0.12	0.11	-8.4
Sport (1350 RPM)	-0.036	-0.12	0.11	-10.0

The magnitude frequency responses for RPM and pitch control of the yaw axis are shown in Figs. 16 & 17, respectively. Considering RPM control, the frequency response magnitude is not significantly impacted by the operating point, as the motor dynamics are not very sensitive to their operating state. With pitch control, the gain is higher for higher trim rotor speed due to the increase in torque's sensitivity to collective pitch, T_Θ.

The frequency response phase for RPM and pitch control are shown in Fig. 18. As in the other axes, the trim point does not substantially affect the phase response, and the both control strategies are dominated by the rigid body dynamics at very low frequency. However, unlike the thrust-dominated axes, there is substantially more phase lead in the mid- to high-frequency range when using RPM control. This is primarily due to the direct effect that voltage has on yaw rate, represented by the zero in Eq. 23, which also prevents additional phase roll off at high frequency.

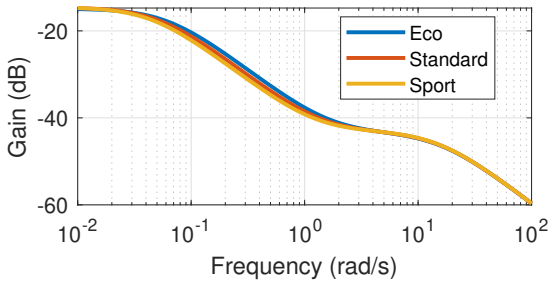

Figure 16: Magnitude Frequency Response of Motor Voltage Input to Yaw Rate ($|r/V_d|$)

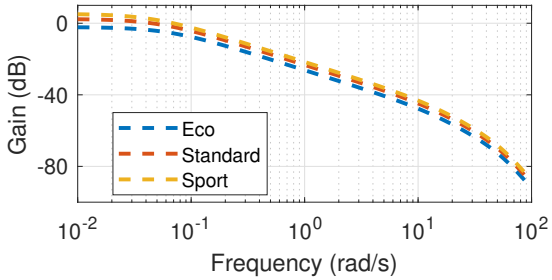

Figure 17: Magnitude Frequency Response of Blade Pitch Input to Yaw Rate ($|r/\Theta_{d,cmd}|$)

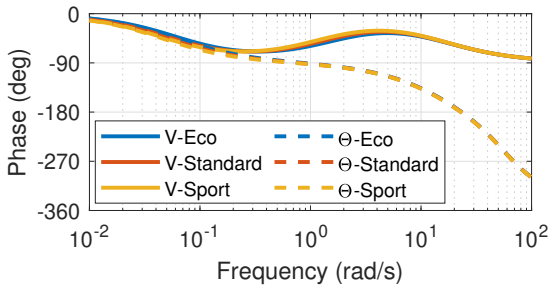

Figure 18: Phase Frequency Response of Differential Input to Yaw Rate ($\angle r/V_d$ and $\angle r/\Theta_{d,cmd}$)

Pure RPM and Pitch Control

Before hybrid control is considered, the aircraft response is examined with pure RPM control or pure pitch control through a series of time domain simulations of the system linearized about the three hover trim points. These simulations are used to examine the transient response of the aircraft with controllers designed to meet 70% of the maximum achievable design margin.

Heave The first simulation is a heave step response. The design margins used for each trim point and control strategy are listed in Table 8.

No design margin is implemented on the Eco trim point with pitch control, since this operating point was defined using the minimum stall margin that allowed satisfactory heave handling qualities. With increasing trim rotor speed, the design margin for pitch control increases as a result of the increased stall margin as well as the increased sensitivity to changes in pitch (Table 5).

The design margin with RPM control shows the opposite trend as pitch control, with decreasing design margin at higher trim rotor speeds as a result of increased current. This trend is also reflected in the decreasing sensitivity of heave rate to changes in rotor speed seen in Table 5.

Table 8: Design Margin Optimization on Heave Axis

Mode	Design Margin	Limit
Sport - Ω	0.4	Max Current
Sport - Θ	1.5	OLOP (disturbance)
Standard - Ω	0.7	Max Current
Standard - Θ	1.1	OLOP (disturbance)
Eco - Ω	1.0	OLOP (disturbance)
Eco - Θ	0	Max Blade Pitch

It is worth noting here that the DMO reaches the current limit around a similar design margin as OLOP reached the limit of satisfactory values. Since the rate limit imposed for the OLOP specification limits the rotor acceleration based on the same maximum current, this suggests that the OLOP specification boundaries may be sufficient in approximating when the current may be saturated during a step response when using rotor speed control.

The aircraft is commanded to reach a climb rate of 3.8 m/s (590 ft/min) at time $t = 1$ second and responses are shown in Fig. 19. The differing rise times seen in Fig. 19 demonstrate the increased responsiveness that comes with higher design margin during control design.

The collective rotor speeds and blade pitches during the heave rate step are shown in Fig. 20. The feedback control on the rotor speed keeps it at the trim value when using pitch control (solid lines), while an increase in blade pitch produces the additional thrust to accelerate the aircraft. When using RPM control (dashed lines), the rotor speed changes to produce more thrust, while the pitch stays the same.

The power to a single motor during the heave simulation is shown in Fig. 21. As expected, RPM control requires significant spikes in power (and current) in order overcome rotor inertia and accelerate the rotors in order to quickly produce the change in thrust needed to begin climb. These spikes are not seen in the pitch control cases since this control strategy only needs to overcome aerodynamic torque. This suggests that pitch control is better for thrust-driven maneuvers, since it requires smaller bursts of power to produce changes in thrust. At lower trim rotor speed (Eco Mode), pitch control is not able to achieve as fast a response as RPM control, since this mode trades stall margin and speed of response for reduced power. The reverse is true for Sport mode, which has higher trim power, but also the fastest response.

Yaw Table 9 shows the design margin achieved in the yaw axis for each trim point and control strategy. Due to the low sensitivity of rotor torque to rotor pitch, Θ-based control strategies were typically inferior to Ω-based control strategies, since the pitch actuators tended to reach their maximum positions during yaw commands. This was not captured during the control design phase due to the lack of position constraints in Table 3, but could be captured during the optimization by including a time domain specification on the max yaw rate.

Table 9: Design Margin Optimization on Yaw Axis

Mode	Design Margin	Limit
Sport - Ω	0.4	OLOP (disturbance)
Sport - Θ	0.4	Max Blade Pitch
Standard - Ω	0.6	OLOP (disturbance)
Standard - Θ	0	Max Blade Pitch
Eco - Ω	0.7	OLOP (disturbance)
Eco - Θ	0	Max Blade Pitch

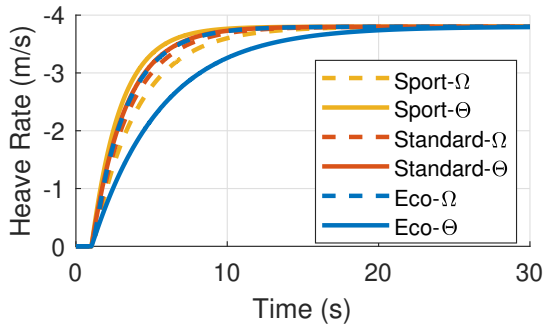

Figure 19: Heave Response with pure RPM or Pitch Control

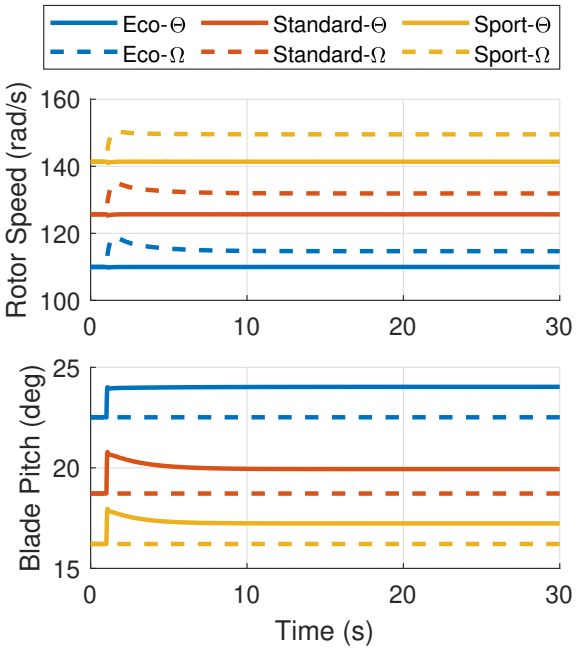

Figure 20: Blade Pitch and Rotor Speed During Heave Response with pure RPM or Pitch Control

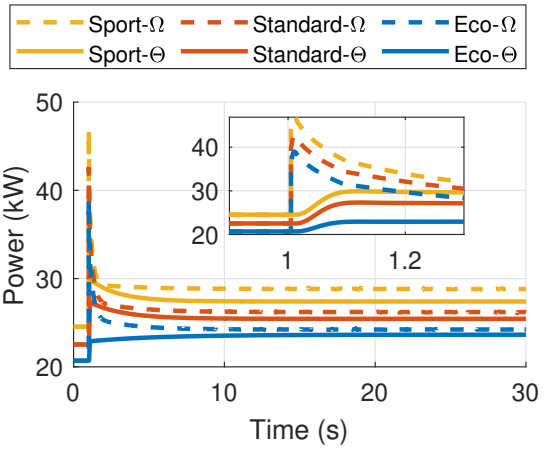

Figure 21: Single Motor Power During Heave Response with pure RPM or Blade Pitch Control

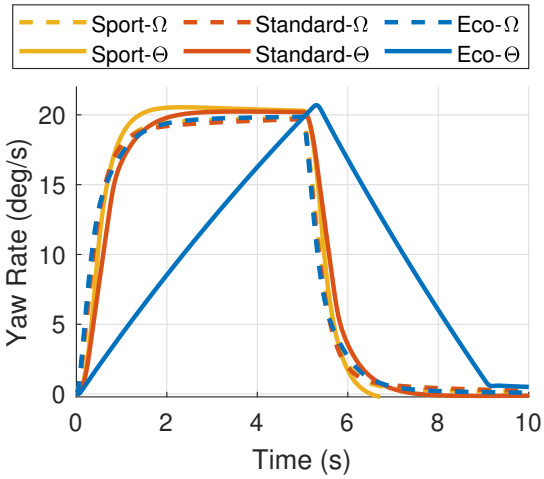

Figure 22: Yaw Response with pure RPM or Pitch Control with DMO

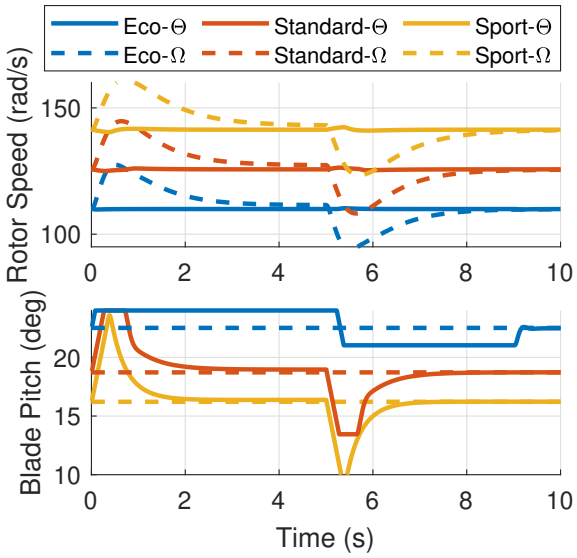

Figure 23: Rotor Speed and Blade Pitch During Yaw Response with Pure RPM/Pitch Control with DMO

A 20 deg/s command in yaw rate is held for 5 seconds, with responses shown in Fig. 22. With the exception of pitch control in Eco mode, similar performance is shown at all trim points and control strategies. With pitch control in Eco-mode, however, the pitch actuator position is limited by the maximum blade pitch imposed to avoid stall. As a result, the maximum yaw acceleration is severely limited, preventing the system from following the first-order command model. Thus, it can be concluded that exclusive pitch control is not feasible for this configuration in yaw.

Figure 23 shows the rotor speed and pitch commands during the yaw step. Due to the fact that the motor dynamics are insensitive to the trim condition, the rotor speed during the yaw step is identical for all three trim points, except for a constant offset. The pitch inputs, however, are characterized by both rate and position saturation, even in sport mode. Due to this, and the lack of substantial performance improvements, the use of collective pitch for yaw control is not recommended when reaction torque is used to control the vehicle.

Hybrid Control

Thus far, it has been concluded that pitch control is more effective for the thrust-driven roll, pitch, and heave axes, while RPM control is better for the torque-driven yaw axis. Now, pitch control will be compared to hybrid control for heave and pitch responses at the Standard (1200 RPM) trim point. A cutoff frequency of 1 rad/s is chosen for the complementary filter of the hybrid controller. The feedback controllers optimized for the purely pitch-based controllers are applied to the hybrid controller, since its short-term responses, on which the specifications in Table 3 are based, are governed by the pitch actuators.

Heave Rate Step A step in heave rate is simulated on the aircraft model linearized about the "Standard" trim point with hybrid control (Fig. 24). With a design margin of 1.4, the heave response is the same with the hybrid and pitch controllers, as expected.

The power consumption during the heave simulation with hybrid control is shown in Fig. 25. The initial spike in power seen with RPM control (Fig. 21) become less severe as the pitch actuator is used to generate the initial thrust increment to enter climb, as less current is needed when the rotor is allowed to accelerate more slowly. With $\alpha = 1$ rad/s, the initial

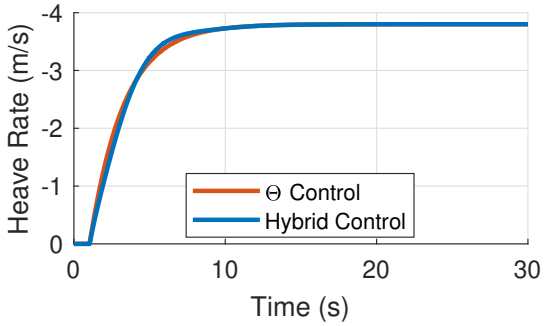

Figure 24: Heave Response with Hybrid Control

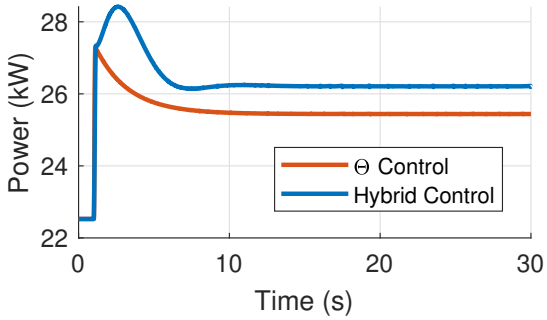

Figure 25: Single Motor Power During Heave Response with Hybrid Control

heave acceleration requires slightly more motor power than pitch control. As the rotor speed settles to a higher trim value, the power remains higher with hybrid control as a result of higher voltage needed to maintain the rotor speed. This implies that pure pitch control is more power efficient for climb, as was found in Ref. 8.

Hybrid Control for Payload Change Though Fig. 25 implies that pure pitch control is more power efficient for climb commands, the benefits of hybrid control for heave can be demonstrated by considering changing trim conditions in simulations of the nonlinear model with either pure pitch or hybrid ($\alpha = 1$ rad/s) control. Consider a case of payload drop-off where the weight of the vehicle is suddenly reduced by 80 kg (15% gross weight) at $t = 1$ second (e.g. releasing a slung load in hover). Shown in Fig. 26, this sudden change in weight causes the aircraft to initially accelerate upward before returning to hover. The response is essentially the same for either control type.

The rotor speed and blade pitch inputs during the payload drop-off are shown in Fig. 27. With pitch control, the collective blade pitch initially decreases in order to reduce the thrust. It then stays at a lower value as a new trim condition with lower thrust is reached. With hybrid control, the collective blade pitch initially decreases in order to quickly reduce thrust, but then returns to its nominal value as the rotor speed slows.

The fact that the aircraft becomes 80 kg lighter naturally reduces the power required to hover, regardless of control strategy. However, the power reduction is 24.3% greater when hybrid control is used instead of pure pitch control, resulting in a 5.0% lower trim power at the reduced aircraft weight. The additional power consumed by the pitch-based controller does have a benefit though. Because the rotor is operating at a higher speed and lower collective pitch, it has additional stall margin, relative to the hybrid controller, but this excess stall margin does not affect the command filters or feedback gains, so no piloted or disturbance rejection bandwidth is gained. Thus, the hybrid controller can afford to trade the excess stall margin for reduced power consumption.

Conversely, if additional payload is acquired, rather than dropped off, the hybrid controller will increase power by a greater margin than the purely pitch-based controller. However, the lower power consumed using the pitch-based controller comes at the cost of stall margin, which may result in hitting pitch limits if maneuvers are executed while carrying the extra payload. The hybrid controller mitigates this risk by consuming more power to maintain a certain stall margin in hover.

Pitch Attitude Doublet The pitch response with hybrid control is analyzed using a doublet input in pitch attitude simulated using the linear model, again in standard mode. This input commands the aircraft to pitch 10 degrees nose up for 5 seconds and then 10 degrees nose down for 5 seconds before returning to hover. This produces the maximum change in

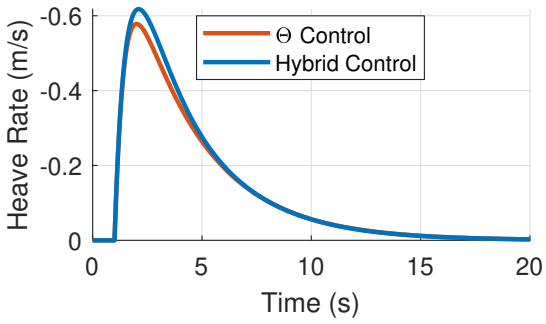

Figure 26: Heave Rate with Payload Drop-Off

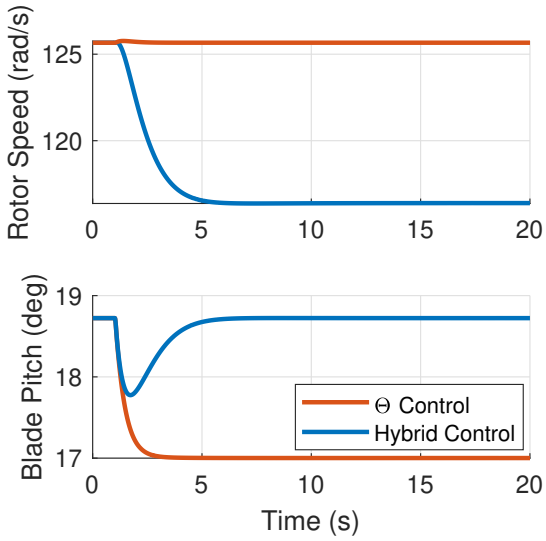

Figure 27: Collective Control Inputs with Payload Drop-Off

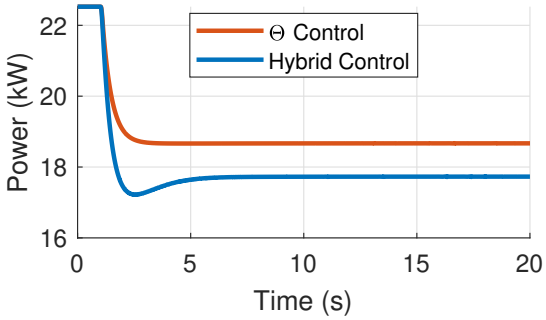

Figure 28: Power with Payload Drop-Off

commanded pitch attitude of 20 degrees. The feedback control gains and command filters corresponding to the design-margin-optimized pitch-based controller are applied to both the hybrid and pitch controllers.

The aircraft response to the pitch doublet is the same regardless of control type (Fig. 29). The rotor speed and blade pitch of rotor 1 during the doublet are plotted in Fig. 30. Small changes in rotor speed are visible with pitch control before the RPM feedback brings the rotor speed back to the trim value. Due to the ACAH control type, the aircraft translates slowly at

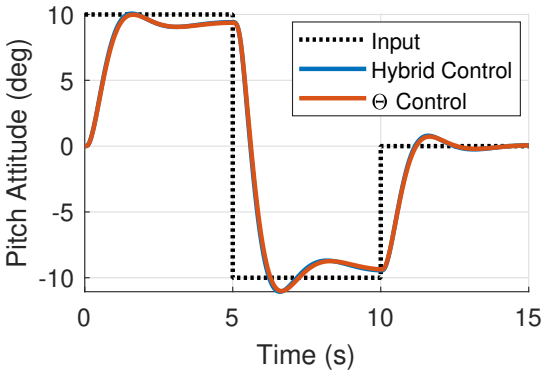

Figure 29: Response to Pitch Doublet Input with Pitch and Hybrid Control

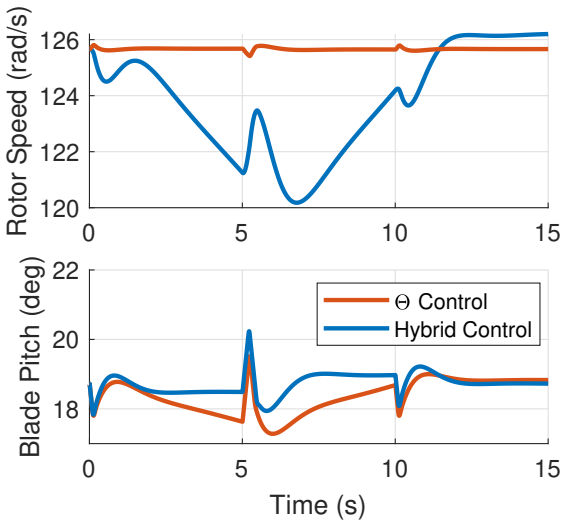

Figure 30: Rotor 1 Speed and Blade Pitch During Pitch Doublet

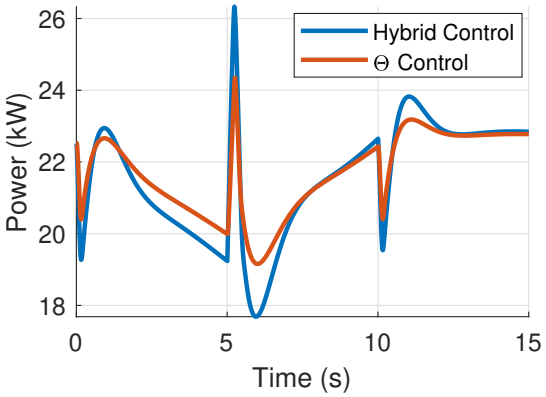

Figure 31: Rotor 1 Power During Pitch Doublet

the end of the simulation (no feedback on velocity is present), resulting the in rotor speed settling to a slightly different trim value when using hybrid control, and the blade pitch to be slightly higher when using pitch control.

The power to rotor 1 during the pitch doublet is shown in Fig. 31. The pitch and hybrid control require similar small peaks in power to each rotor, through the total power will remain close to the trim value.

Forward Flight As shown by previous work (Ref. 8), using rotor speed to trim in forward flight is more power-efficient than using blade pitch. This is a key benefit that hybrid control provides over pitch control alone.

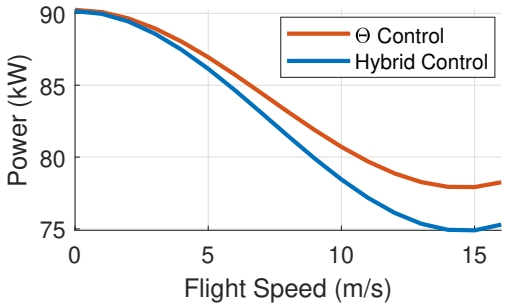

Figure 32: Trim Power in Forward Flight

Fig. 32 shows the difference in power between using the rotor speeds to trim in forward flight (with the blade pitches held at hover values) versus using blade pitch to trim in forward flight (with rotor speeds held at hover trim values). At a flight speed of 15 m/s (30 knots), the use of hybrid control to trim provides a 3.9% reduction in trim power compared to pitch control alone.

DISCUSSION

A quadcopter with both variable rotor speed and variable collective pitch on each rotor was simulated in hover. Through hover trim analysis it was found that having both motor voltage and blade pitch available as control inputs allows a choice of trim point. Generally speaking, operation at lower RPM was found to be associated with lower power consumption and reduced stall margin.

The choice of trim point affects the dynamics of the aircraft. The linear dynamics of the aircraft were broken down into simplified transfer functions for each axis and control input. Analyzing the hover dynamics at three different trim points, increased trim rotor speed increased the sensitivity of thrust-driven responses to changes in collective pitch but reduced sensitivity to RPM changes.

Two key differences between the torque-driven yaw dynamics and thrust-driven axes were identified. First, the blade pitch inputs have no direct effect on the yaw acceleration. Rather, they influence the yaw rate indirectly through the motor dynamics. Second, changes in motor voltage have both a direct effect on yaw acceleration and an indirect effect via rotor acceleration. Thus, the motor dynamics can be represented by a pole-zero pair, resulting in lead-lag behavior, rather than a simple lag, as was observed for the thrust-dominated axes.

The observed differences in dynamics, as well as the differences in stall margin, affect the achievable design margins when considering pure RPM- or pitch-control at the different trim points. Similar to the trends in control derivatives, the heave design margin increases with higher trim rotor speed when using pitch-control, but decreases with RPM-control. It was also observed that the use of pitch control for heave acceleration eliminates the power spikes associated with initial acceleration of the rotors.

When considering pure RPM or pitch control for the torque-driven yaw axis, pitch control (and by extension, hybrid control) provides no advantage over RPM control for the uncanted rotors considered in this study. With pure pitch control, two of the trim points (Eco and Standard) were unable to provide satisfactory yaw response without pitch actuator saturation.

As the handling qualities requirements were incrementally increased during design margin optimization, it was observed that both OLOP and direct current limits reached the bound of acceptability at similar design margins when RPM-control was used, supporting the use of OLOP to limit the current drawn by any given motor.

The use of a complementary filter for hybrid control mixing routes high-frequency (maneuver) input content to the pitch actuator and low-frequency (trim) input content to rotor speed commands. Through consideration of different complementary filter cutoff frequencies and motor time constants, it was found that the motor time constant should be limited to a maximum of one-tenth the filter frequency in order to avoid giving commands to the motors that they cannot adequately follow. When using primarily pitch control for maneuvers, the value of the motor time constant time can be fixed to $0.1/\alpha$ with no impact on the vehicle dynamics, as the low-pass filter dominates over the closed-loop motor dynamics. For model inversion, the equivalent delay was found to be driven by the pitch actuator and can be fixed to a constant value as long as $\alpha \leq 1/\tau_\Omega$.

Hybrid control allows the benefits of pitch control for maneuvers with the trim benefits of RPM control in steady-state operation. Through comparison of hybrid control to pitch control it was shown that hybrid control of the heave axis can provide the same response with similar transient power while recovering the same stall margin in trim. From simulation of a drop-off of payload weight, hybrid control provided a 5.0% reduction in trim power compared to pitch control. For the roll/pitch axis, the same response was achieved with either hybrid or pitch control with similar motor power. Finally, trim in forward flight was considered, where hybrid control achieved 3.9% lower trim power than pitch control at a flight speed of 15 m/s (30 knots).

CONCLUSIONS

Several key conclusions are drawn from the examination of the hover dynamics and flight control of the UAM-scale quadcopter with hybrid RPM/pitch control presented in this study. In summary, it is concluded that:

- By operating at higher trim rotor speed and lower blade pitch in hover trim, increased trim power can be traded for greater maneuverability as a result of increased stall margin and sensitivity to pitch inputs when considering thrust-driven responses.
- The torque-driven yaw dynamics differ from the other axes, and hybrid control offers no benefit over RPM control for yaw maneuvers.
- The use of a complementary filter routes high-frequency input content to the pitch actuators and low-frequency input content to changes in rotor speeds, allowing the aircraft to utilize the faster response of the pitch actuators for maneuvers while still gaining the benefits of utilizing changes in rotor speeds to trim.
- For thrust-driven maneuvers, hybrid control eliminates the spikes in power needed to overcome rotor inertia when using RPM-control alone by quickly producing changes in thrust with blade pitch actuators.

Author contact:
Ariel Walter: waltea@rpi.edu
Michael McKay: michael.mckay005@gmail.com
Robert Niemiec: niemir2@rpi.edu
Farhan Gandhi: fgandhi@rpi.edu

ACKNOWLEDGMENTS

This work is carried out at Rensselaer Polytechnic Institute under the Army/Navy/NASA Vertical Lift Research Center of Excellence (VLRCOE) Program, grant number W911W61120012, with Dr. Mahendra Bhagwat as Technical Monitor. The authors would like to acknowledge the Army Combat Capabilities Development Command for sponsoring Ms. Walter through the SMART Scholarship Program.

REFERENCES

1. Walter, A., McKay, M., Niemiec, R., Gandhi, F., and Ivler, C., "Hover Handling Qualities of Fixed-Pitch, Variable-RPM Quadcopters with Increasing Rotor Diameter," VFS International 76th Annual Forum, Virtual, October 6–8, 2020.
2. Bahr, M., McKay, M., Niemiec, R., and Gandhi, F., "Handling Qualities Assessment of Large Variable-RPM Multi-Rotor Aircraft for Urban Air Mobility," VFS International 76th Annual Forum, Virtual, October 6–8, 2020.
3. Malpica, C., and Withrow-Maser, S., "Handling Qualities Analysis of Blade Pitch and Rotor Speed Controlled eVTOL Quadrotor Concepts for Urban Air Mobility," VFS International Powered Lift Conference 2020, San Jose, CA, January 21–23, 2020.

4. Withrow-Maser, S., Malpica, C., and Nagami, K., "Multirotor Configuration Trades Informed by Handling Qualities for Urban Air Mobility," 76th Annual VFS Forum, Virtual, October 6–8, 2020.

5. Niemiec, R., Gandhi, F., Lopez, M., and Tischler, M., "System Identification and Handling Qualities Predictions of an eVTOL Urban Air Mobility Aircraft Using Modern Flight Control Methods," 76th Annual VFS Forum, Virginia Beach, VA, October 6–8, 2020.

6. Theron, J. P., Horn, J., Wachpress, D., and Enciu, J., "Nonlinear Dynamic Inversion Control for Urban Air Mobility with Distributed Electric Propulsion," VFS International 76th Annual Forum, Virtual, October 6–8, 2020.

7. "Aeronautical Design Standard, Performance Specification, Handling Qualities Requirements for Military Rotorcraft," Technical Report ADS-33E-PRF, March 2000.

8. McKay, M., Niemiec, R., and Gandhi, F., "Performance Comparison of Quadcopters with Variable-RPM and Variable-Pitch Rotors," *Journal of the American Helicopter Society*, Vol. 64, 2019.

9. Walter, A., Niemiec, R., and Gandhi, F., "Effects of Disk Loading on Handling Qualities of Large-Scale, Variable-RPM Quadctopers," VFS International 77th Annual Forum, Palm Beach, Florida, May 11–13, 2021.

10. Johnson, W., Silva, C., and Solis, E., "Concept Vehicles for VTOL Air Taxi Operations," AHS Technical Conference on Aeromechanics Design for Transformative Flight, San Francisco, CA, January 16–18, 2018.

11. Niemiec, R., and Gandhi, F., "Development and Validation of the Rensselaer Multicopter Analysis Code (RMAC): A Physics-Based Comprehensive Modeling Tool," 75th Annual VFS Forum, Philadelphia, PA, May 13–16, 2019.

12. Peters, D., Boyd, D., and He, C. J., "Finite-State Induced-Flow Model for Rotors in Hover and Forward Flight," *Journal of the American Helicopter Society*, Vol. 34, (4), 1989, pp. 5–17.

13. Niemiec, R., and Gandhi, F., "Multi-rotor Coordinate Transform for Orthogonal Primary and Redundant Control Modes for Regular Hexacopters and Octocopters," 42nd European Rotorcraft Forum, Lille, France, September 5–8, 2016.

14. Tischler, M., Berger, T., Ivler, C., Mansur, M., Cheung, K., and Soong, J., *Practical Methods for Aircraft and Rotorcraft Flight Control Design: An Optimization-Based Approach*, AIAA Education Series, Reston, VA, 2017.

15. Walter, A., McKay, M., Niemiec, R., Gandhi, F., Hamilton, C., and Jaran, C., "An Assessment of Heave Response Dynamics for Electrically Driven Rotors of Increasing Diameter," Autonomous VTOL Technical Meeting & eVTOL Symposium, Mesa, AZ, January 28–31, 2019.

16. Tischler, M., and Remple, R., *Aircraft and Rotorcraft System Identification: Engineering Methods with Flight Test Examples*, AIAA Education Series, Reston, VA, 2012.

17. Berger, T., Ivler, C., Berrios, M., Tischler, M., and Miller, D., "Disturbance Rejection Handling-Qualities Criteria for Rotorcraft," 72nd Annual AHS Forum, West Palm Beach, FL, May 16–19, 2016.